Journal of Computational Physics 229 (2010) 325–342

Contents lists available at ScienceDirect

Journal of Computational Physics

journal homepage: www.elsevier.com/locate/jcp

Slow-time acceleration for modeling multiple-time-scale problems

A. Haselbacher [a,*], F.M. Najjar [b,1], L. Massa [b,2], R.D. Moser [c]

[a] Department of Mechanical and Aerospace Engineering, University of Florida, Gainesville, FL 32611-6300, United States
[b] Center for Simulation of Advanced Rockets, University of Illinois at Urbana-Champaign, Urbana, IL 61801, United States
[c] Department of Mechanical Engineering and Institute for Computational Engineering and Sciences, University of Texas at Austin, Austin, TX 78712, United States

ARTICLE INFO

Article history:
Received 5 February 2008
Received in revised form 3 August 2009
Accepted 23 September 2009
Available online 4 October 2009

Keywords:
Multi-scale problems
Stiff problems
Asymptotic analysis
Slow-time acceleration
Implicit methods

ABSTRACT

The numerical simulation of a system exhibiting a broad range of time scales can be very expensive because the time discretization will in general need to resolve the smallest time scale, and the simulation will have to extend over many times the longest time scale. However, it is common that not all the time scales are of interest for a particular problem. When the long time scales are of primary interest, a number of techniques are available to eliminate the unwanted short time scales from consideration. When the short time scales are of primary interest, a technique for mitigating the consequences of anomalously long time scales is needed. The "slow-time acceleration" technique presented here has been developed to address this problem. In the slow-time acceleration technique, a modified evolution equation is developed in which the longest time scale is much shorter than that of the original system, and which has the same multi-time scale asymptotic structure as the original system. As an example, this approach is applied to the numerical simulation of solid-propellant rockets in which the long time scale is associated with the regression of the burning propellant.

1. Introduction

Many problems in science and engineering are characterized by multiple spatial and/or temporal scales. Some well-known simple examples include laminar and turbulent shear layers and chemically reacting flows with widely varying reaction rates.

There is a subcategory of such problems in which the dominant dynamical processes governing the phenomena occur on time scales that are much faster than the evolution of bulk system features. Just a few examples of this class of multi-time scale problems include:

- The slow evolution of a river compared to the turbulent fluid-dynamics that govern erosion and deposition of sediments, see, e.g., Best [3].
- The slow evolution of a protein configuration compared to the dynamics of atomic motion responsible for the configuration changes, see, e.g., Pande et al. [14].
- The slow maneuvering of an aircraft compared to the fluid-dynamic processes in the shear layers on the aircraft's wings.

* Corresponding author. Address: Department of Mechanical and Aerospace Engineering, University of Florida, 222 MAE-B, P.O. Box 116300, Gainesville, FL 32611-6300, United States. Tel.: +1 352 392 9459; fax: +1 352 392 1071.
E-mail addresses: haselbac@ufl.edu (A. Haselbacher), najjar2@llnl.edu (F.M. Najjar), massa@uta.edu (L. Massa), rmoser@ices.utexas.edu (R.D. Moser).
[1] Present address: Lawrence Livermore National Laboratory, 7000 East Avenue, L-500, Livermore, CA 94551, United States.
[2] Present address: Mechanical and Aerospace Engineering Department, The University of Texas at Arlington, Arlington, TX 76019, United States.

0021-9991/$ - see front matter © 2009 Elsevier Inc. All rights reserved.
doi:10.1016/j.jcp.2009.09.029

- The slow regression of the propellant in a solid-propellant rocket compared to the dynamics of the chemical and fluid-dynamic processes responsible for the regression, see, e.g., Sutton and Biblarz [18].

In these phenomena, the dominant fast-scale processes acting over long periods of time produce the slow evolution of the system, and as the system evolves on the slow time scale, the properties of the fast-scale dynamics change.

Widely disparate time scales can be treated via multi-scale asymptotics (see, e.g., Holmes [10] and Bender and Orszag [2]), but usually the simplified asymptotic problem is analytically intractable and therefore requires numerical solution. Alternatively, a straightforward direct numerical simulation of the slow scales requires evolving the fast scales over long times. The cost of the simulation is thus proportional to τ_s/τ_f, where τ_s and τ_f denote the slowest and fastest time scales, respectively. This cost can be prohibitive if τ_s and τ_f differ by many orders of magnitude, making simulations unattractive or infeasible. In this paper, we propose a solution strategy, or more precisely a numerical modeling strategy, for such problems that allows accelerating the slow time scale and therefore makes numerical simulations feasible.

During the development of this approach, the system of interest was the last in the above list, namely a solid-propellant rocket motor (SRM). To describe the problem the slow-time acceleration approach is intended to solve, the practical issues facing the numerical solution of an SRM are briefly explained here. The fundamental problem is that the flow in SRMs exhibits a wide range of spatial and temporal scales. The spatial scales range from aluminum-oxide particles with a diameter of about 3 μm to the overall length of the motor of about 40 m for the Space Shuttle Reusable Solid Rocket Motor (RSRM). A detailed discussion of the range of time scales is presented by Haselbacher et al. [9]. Here it is sufficient to note that the fastest physical time scale is of the order of 10^{-6} s while the slowest physical time scale is the time to burn-out of the solid propellant, which is about 120 s for the RSRM. The wide range of length and time scales makes detailed first-principle simulations of SRMs from ignition to burn-out, such as those undertaken at the Center for Simulation of Advanced Rockets (CSAR, see Dick et al. [4]), very challenging. In such simulations, evolution equations are solved for the mass, momentum, and energy of the mixture of gaseous species and aluminum-oxide smoke and for the aluminum droplet position, mass, momentum, energy, and composition (see, e.g., Najjar et al. [13] and Haselbacher and Najjar [8]). The simulations are detailed in the sense that all relevant physical processes are included (e.g., turbulence and aluminum droplet combustion), and modeled as accurately as possible from first principles.

In addition to the physical time scales discussed above, numerical time scales may be introduced due to stability limitations of explicit time-integration methods. In some problems, e.g., the computation of forces and moments due to the flow over wings slowly oscillating in pitch, the stability time scale can be many orders of magnitude smaller than the fastest physical time scales. In this case, it is appropriate to relieve the stability restriction by using an implicit time-integration scheme, see, e.g., Jameson [11] and Pulliam [15]. However, when the physical time scales are too short to allow practical numerical solutions, other approaches are needed. For example, to avoid the fast acoustic time scale in weakly compressible flows, either the incompressible or preconditioned compressible Navier–Stokes equations, see, e.g., Turkel [22], are often solved. For the same reasons, low-speed reacting flows are usually treated with the zero-Mach-number equations, see Rehm and Baum [16] and Majda and Sethian [12]. In the context of multi-phase flows, Ferry and Balachandar [5] developed the Equilibrium-Eulerian method to eliminate the time scales associated with the dynamics of very small particles. In all of these cases, short time scales that are not of interest (numerical or physical) are removed. It is important to note that our approach addresses a different situation: In the problems addressed here, the short time scales are of primary interest and anomalously long time scales are causing problems.

Here a new method designed specifically to treat problems with an anomalously large time scale, such as an SRM, is presented. This new method, called "slow-time acceleration," is based on an asymptotic analysis of the governing equations and is described in detail in Section 2. This method allows for the acceleration of a slow time scale while leaving the dynamics of the fast time scale unchanged. The general principles of slow-time acceleration are illustrated by applying it to linear and non-linear damped oscillators in Section 2.2.

The slow-time acceleration technique is applied here to a model of an SRM to demonstrate both its potential and the challenges involved. A simplified SRM model is considered that does not include many of the complicating physical processes present in real SRMs, such as turbulence, multi-phase flow, so-called "erosive burning," and ignition. Many of these processes act on fast time scales, and indeed an interest in simulating them motivated the development of the acceleration technique proposed here. These processes are omitted from the demonstration problem so that simulations without slow-time acceleration remain feasible, although other fast time-scale processes are still present. Such unaccelerated simulations will be used for comparison. The slow-time acceleration method is derived for our SRM model in Section 3, and the acceleration achieved by the method for the SRM model is demonstrated in Section 4. Conclusions and suggested further developments are presented in Section 5.

2. Slow-time acceleration

Slow-time acceleration is intended for systems that exhibit multiple time-scale behavior, with at least one very large time scale, and for which the dynamics of the fast time scales are of primary interest. The goal is to accelerate the evolution of the slow time scale while preserving the dynamics of the fast time scale.

2.1. General formulation

To illustrate slow-time acceleration, consider the general system

$$\frac{\partial \phi}{\partial t} = \mathcal{N}(\phi, t; \epsilon), \tag{1}$$

where $\mathcal{N}$ is some nonlinear operator that depends on the small parameter ϵ, and this dependence is assumed to lead to multi-scale behavior. In particular, the slow time scale is assumed to be $1/\epsilon$ of the fast time scale. Following the notation of Bender and Orszag [2] for multi-scale asymptotic analysis, the slow-time variable $T = \epsilon t$ is introduced. The solution ϕ is taken to depend on both the fast- and slow-time variables independently, where the fast-time variable is now denoted by t. The time derivative in Eq. (1) is then transformed to yield

$$\frac{\partial \phi}{\partial t} + \epsilon \frac{\partial \phi}{\partial T} = \mathcal{N}(\phi, t; \epsilon). \tag{2}$$

To accelerate through the slow time scale, it must be shortened by a factor of $\beta > 1$. Then the slow time scale will be $1/\beta\epsilon$ times the fast time scale. This could be accomplished by substituting $\beta\epsilon$ for ϵ in Eq. (1), but in general this will also affect the fast time-scale dynamics. Instead, a modified form of Eq. (1) is sought,

$$\frac{\partial \phi}{\partial t} = \mathcal{N}^{\beta}(\phi, t; \epsilon), \tag{3}$$

where the nonlinear operator $\mathcal{N}^{\beta}$ is a modification of $\mathcal{N}$ such that when ϵ is replaced by $\beta\epsilon$, the corresponding multi-scale equation

$$\frac{\partial \phi}{\partial t} + \beta\epsilon \frac{\partial \phi}{\partial T} = \mathcal{N}^{\beta}(\phi, t; \beta\epsilon) \tag{4}$$

will be identical to Eq. (2), i.e.,

$$\mathcal{N}^{\beta}(\phi, t; \epsilon) = \mathcal{N}(\phi, t; \epsilon/\beta) + \frac{\beta - 1}{\beta} \epsilon \frac{\partial \phi}{\partial T}. \tag{5}$$

Provided $\beta\epsilon \ll 1$, Eq. (4) can be used in place of the original equation, for example in numerical simulations. The short-time behavior of the solution (i.e., the rate of rapid oscillations) is then the same as that of the original, but a factor of β shorter simulation can be employed to cover the long-term behavior of the solution. If one is interested in the short-time behavior of the solution of the original system (without slow-time acceleration) in the neighborhood of some large time $t^* \gg 1$, one would examine the solution of the accelerated system in the neighborhood of time t^*/β. The short-time evolution will be identical.

Two important points must be made about the slow-time acceleration approach. First, the goal of slow-time acceleration is different from that of standard multi-scale asymptotic analysis. In the latter, one seeks to develop an approximate solution to the problem at hand by exploiting the multi-scale asymptotic structure of the problem. In slow-time acceleration, however, we seek to develop modified equations describing the problem that will facilitate numerical simulation by speeding up slowly evolving processes. We require the modified equations to have the same multi-scale asymptotic structure as the original equations. That is, if we were to apply a classical multi-scale asymptotic analysis to the original and modified set of equations, the results should be identical. Many of the issues that arise in multi-scale asymptotic analysis (treatment of secular terms, solvability and regularity conditions, etc.) do not occur in the development of slow-time acceleration because the asymptotic solution process is never carried out. However, in slow-time acceleration, it is still necessary to identify the time scales to be used in the formulation. In many problems, including the examples described here, appropriate time scales are easily identified. In other problems, the time scales may not be obvious and may need to be identified by an asymptotic analysis. In essence, slow-time acceleration requires knowledge of the multi-scale asymptotic characteristics of the problem that will be preserved. Also required are approximations for the slow-time derivatives that appear explicitly in the accelerated equations (see Eq. (5)). Such approximations might be accessible through a classical multi-scale analysis. However, more commonly in complex physical systems such as an SRM, the slow-time derivatives will need to be modeled. Similar multi-scale modeling approaches have been adopted by Spalart [17] and Venugopal et al. [23].

Second, it is important to note a fundamental difference between implicit methods and the slow-time acceleration approach. In implicit methods, the goal is to either relieve or remove a numerical stability limit. Thus, one may view the effect of implicit methods as shifting fast numerical time scales toward the slower physical time scales of primary interest. In contrast, in the slow-time acceleration method, slow physical time scales are brought closer to the fast physical time scales of primary interest. In the case of the SRM problem used as an example in this article, the slow time scales are those associated with the pressurization of the chamber and the burn-back of the propellant. The fluid-dynamic time scales of primary interest are much shorter as discussed in Section 3.1. A schematic of the intended effect of slow-time acceleration for this problem is shown in Fig. 1. The volume-filling time scale indicated in the figure is defined as the time constant associated with the equilibration of the average chamber pressure, see Section 3.1.

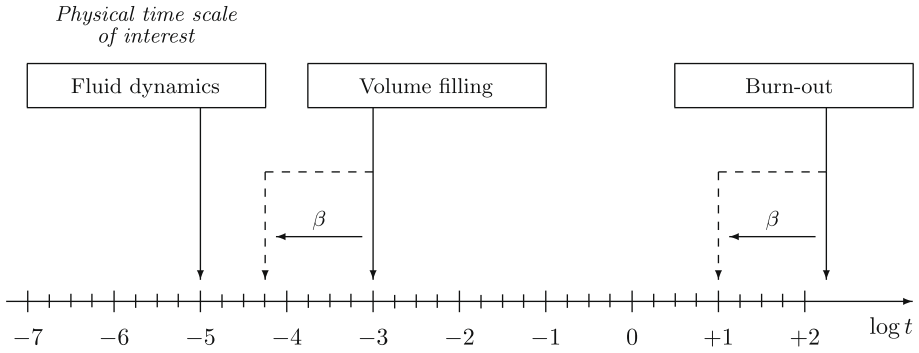

Fig. 1. Schematic effect of acceleration of physical time scales in simulation of SRM. Note that the magnitude of acceleration indicated by dashed arrows is schematic only and not necessarily indicative of an actual simulation.

Before formulating slow-time acceleration for an SRM, the general approach is illustrated by applying it to simple linear and non-linear damped oscillators.

2.2. Examples

2.2.1. Oscillator with linear damping

Consider the weakly damped oscillator problem, given by

$$\phi'' + \epsilon\phi' + \phi = 0, \quad \phi(0) = 0,\ \phi'(0) = 1, \tag{6}$$

where the superscript $'$ denotes differentiation with respect to time. The analytic solution is easily determined to be

$$\phi(t) = \frac{1}{\sqrt{1-\epsilon^2/4}} e^{-\epsilon t/2} \sin(t\sqrt{1-\epsilon^2/4}), \tag{7}$$

which is clearly characterized by oscillations on the fast scale with a decay in amplitude on the slow scale. To apply the slow-time acceleration approach, rewrite Eq. (7) as a system of first-order equations,

$$\frac{d\phi}{dt} = \psi, \tag{8}$$

$$\frac{d\psi}{dt} = -\epsilon\psi - \phi, \tag{9}$$

with initial conditions $\phi(0) = 0,\ \psi(0) = 1$. For the multi-scale analysis, it is stipulated that $\phi = \phi(t, T)$ where $T = \epsilon t$ represents the slow time scale. Thus,

$$\frac{\partial\phi}{\partial t} + \epsilon\frac{\partial\phi}{\partial T} = \psi, \tag{10}$$

$$\frac{\partial\psi}{\partial t} + \epsilon\frac{\partial\psi}{\partial T} = -\epsilon\psi - \phi. \tag{11}$$

Slow-time acceleration requires that Eqs. (8) and (9) be modified as specified in Eq. (5) so that when ϵ is replaced with $\beta\epsilon$, the multi-scale equations are identical to Eqs. (10) and (11), with the result

$$\frac{d\phi}{dt} = \psi + \frac{\beta-1}{\beta}\epsilon\frac{\partial\phi}{\partial T}, \tag{12}$$

$$\frac{d\psi}{dt} = -\frac{1}{\beta}\epsilon\psi - \phi + \frac{\beta-1}{\beta}\epsilon\frac{\partial\psi}{\partial T}. \tag{13}$$

The multi-scale form of the modified equations is then,

$$\frac{\partial\phi}{\partial t} + \epsilon\frac{\partial\phi}{\partial T} = \psi + \frac{\beta-1}{\beta}\epsilon\frac{\partial\phi}{\partial T}, \tag{14}$$

$$\frac{\partial\psi}{\partial t} + \epsilon\frac{\partial\psi}{\partial T} = -\frac{1}{\beta}\epsilon\psi - \phi + \frac{\beta-1}{\beta}\epsilon\frac{\partial\psi}{\partial T}, \tag{15}$$

and it is clear that when ϵ is replaced by $\beta\epsilon$, the multi-scale form given by Eqs. (14) and (15) is the same as the original multi-scale form given by Eqs. (10) and (11). The equations with accelerated slow time that must be solved are thus (after substituting $\beta\epsilon$ for ϵ)

$$\frac{d\phi}{dt} = \psi + (\beta - 1)\epsilon\frac{\partial\phi}{\partial T}, \tag{16}$$

$$\frac{d\psi}{dt} = -\epsilon\psi - \phi + (\beta - 1)\epsilon\frac{\partial\psi}{\partial T}. \tag{17}$$

The goal is for this system to decay at a rate β times faster than the original system while preserving the same short time-scale behavior.

Eqs. (16) and (17) explicitly involve the slow-time derivatives, so an expression or model for these derivative is required. In simple situations such as this one, the slow derivative can be obtained from the exact solution by noting that the slow decay of the amplitude is the process that occurs on the slow time scale, and so

$$\frac{\partial\phi}{\partial T} = -\frac{1}{2}\phi, \tag{18}$$

$$\frac{\partial\psi}{\partial T} = -\frac{1}{2}\psi. \tag{19}$$

However, normally the exact solution is unknown, so other considerations are required. One possibility is to proceed with a multi-scale asymptotic analysis which yields at first order the result given by Eqs. (18) and (19) for the slow derivatives. Another possibility, which we will pursue here, is to identify a quantity that must evolve primarily on the slow time scale and to use it to identify the slow derivatives. In this case, by examining the equations, we expect the solution to behave as a harmonic oscillator (the $\epsilon = 0$ solution) with slowly varying amplitude $A(T)$. The slow derivative dA/dT must then be determined. To do so, we model $A^2 = \phi^2 + \psi^2$, which is exact for the $\epsilon = 0$ solution, and determine $dA^2/dT = -\psi^2$ from Eqs. (8) and (9). However, it is apparent that this model for A is not perfect because ψ^2 varies on the fast time scale (if $\psi = \cos t$, ψ^2 oscillates between 0 and 1 with frequency 2), which is inconsistent with the amplitude varying slowly. To avoid this problem, we can instead consider the mean value of the amplitude over a period of the fast oscillation (denoted by a bar), which also varies only on the slow time scale. One thus obtains $d\overline{A^2}/dT = -\overline{\psi^2}$, and consistent with the harmonic solution for $\epsilon = 0$, we make the modeling assumptions $\overline{A^2} = 2\overline{\phi^2} = 2\overline{\psi^2}$ and $\overline{A^2} = A^2$. With these approximations, the slow derivatives can be modeled as

$$\frac{d\phi}{dT} \approx \overline{\frac{1}{A}\frac{dA}{dT}}\phi = \frac{1}{2}\overline{\frac{1}{A^2}\frac{dA^2}{dT}}\phi = -\frac{1}{2}\phi, \tag{20}$$

$$\frac{d\psi}{dT} \approx \overline{\frac{1}{A}\frac{dA}{dT}}\psi = \frac{1}{2}\overline{\frac{1}{A^2}\frac{dA^2}{dT}}\psi = -\frac{1}{2}\psi, \tag{21}$$

which are precisely Eqs. (18) and (19). With the slow derivatives modeled by Eqs. (20) and (21), the final equations with accelerated slow time scale are

$$\frac{d\phi}{dt} = \psi - \frac{\beta - 1}{2}\epsilon\phi, \tag{22}$$

$$\frac{d\psi}{dt} = -\phi - \frac{\beta + 1}{2}\epsilon\psi. \tag{23}$$

The analytical solution of these equations is

$$\phi(t) = \frac{1}{\sqrt{1 - \epsilon^2/4}}e^{-\beta\epsilon t/2}\sin(t\sqrt{1 - \epsilon^2/4}), \tag{24}$$

which is identical to Eq. (7) except for the rate of amplitude decay, which is a factor of β faster. This is precisely what was desired. The behavior of the modeled amplitude $A(t)$ for $\beta = 1$ (no acceleration) and $\beta = 10$ is shown in Fig. 2. It can be seen clearly that $A(t)$ for $\beta = 10$ decays ten times faster because when plotted in stretched time t/β, the modeled amplitude matches the unaccelerated result very well.

2.2.2. Oscillator with non-linear damping

To illustrate the application of slow-time acceleration to a non-linear problem, consider the van der Pol equation

$$\phi'' - \epsilon\phi'(1 - \phi^2) + \phi = 0, \tag{25}$$

with $0 < \epsilon \ll 1$ and the initial conditions $\phi(0) = 1$, $\phi'(0) = 0$. Following the steps outlined above for the oscillator with linear damping, the equations with accelerated slow time scale are (after substituting $\beta\epsilon$ for ϵ),

$$\frac{d\phi}{dt} = \psi + (\beta - 1)\epsilon\frac{\partial\phi}{\partial T}, \tag{26}$$

$$\frac{d\psi}{dt} = \epsilon\psi(1 - \phi^2) - \phi + (\beta - 1)\epsilon\frac{\partial\psi}{\partial T}. \tag{27}$$

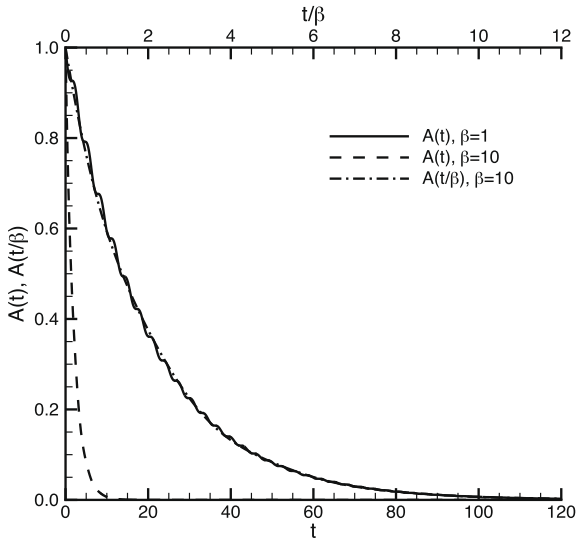

Fig. 2. Comparison of numerical solutions for amplitude A of linear damped oscillator with $\epsilon = 0.1$.

As in the linear oscillator, the solution is expected to be harmonic with slowly varying amplitude, so the slow derivative can be approximated in the same way. Therefore, we model $A^2 = \phi^2 + \psi^2$ and its slow derivative is determined from the governing equations as

$$\frac{dA^2}{dT} = 2\psi^2(1-\phi^2). \tag{28}$$

Also as in the linear case, the model is imperfect, and we resort to averaging to obtain a model derivative that evolves only on the slow scale. In addition to the modeling assumptions used for the linear case, a model for $\overline{\psi^2\phi^2} \approx A^4/8$ is determined from the $\epsilon = 0$ harmonic solution. The average logarithmic slow derivative of A is thus

$$\overline{\frac{1}{A}\frac{dA}{dt}} = \frac{1}{2}\left(1 - \frac{A^2}{4}\right), \tag{29}$$

and the proposed model for the slow derivatives is therefore

$$\frac{\partial\phi}{\partial T} = \frac{1}{2}\left[1 - \frac{1}{4}(\phi^2+\psi^2)\right]\phi, \tag{30}$$

$$\frac{\partial\psi}{\partial T} = \frac{1}{2}\left[1 - \frac{1}{4}(\phi^2+\psi^2)\right]\psi. \tag{31}$$

The numerical solution of Eqs. (26) and (27) with this model is shown in Fig. 3 for $\beta = 1$ (no acceleration) and $\beta = 10$. As expected, the amplitude $A(t)$ primarily evolves slowly compared to the oscillating solution, though there are small fluctuations on the time scale of the oscillation period. In the accelerated computation ($\beta = 10$), the amplitude grows ten times faster, as expected, and when it is stretched in time by plotting $A(t/\beta)$, the curve falls right on the unaccelerated case. When viewed on the fast time scale, see Fig. 3(b), the solution ϕ evolves similarly (same frequency and amplitude) when the normal and accelerated solutions are registered to the same slow time.

2.3. Considerations for modeling of slow derivative

In the oscillator examples discussed above, it is clear *a priori* that it is the amplitude of the oscillations that is evolving slowly. However, this is not the only possibility. For example, in a different oscillator, it might be the frequency of oscillation that was slowly varying (as in the WKB approximation, see Bender and Orszag [2]). More generally, the fast time evolution of the system can occur on a time scale that is itself evolving on the slow time scale. Similarly, in more complex problems governed by partial differential equations (PDEs), the solution my exhibit spatial variations on a length scale that is evolving slowly in time. Ideally, one would have knowledge of these solution characteristics from an asymptotic analysis of the governing equations, as for the oscillators. However, in more realistic models of complex physical systems, it is likely that the nature of the slow-time behavior cannot be determined analytically in a simple manner, but will instead have to be identified through the modeler's physical insight. In either case, to form the basis for a model of the slow derivative, one is seeking to identify quantities (such as an amplitude) that evolve only on the slow time scale. The time derivative of such a quantity is

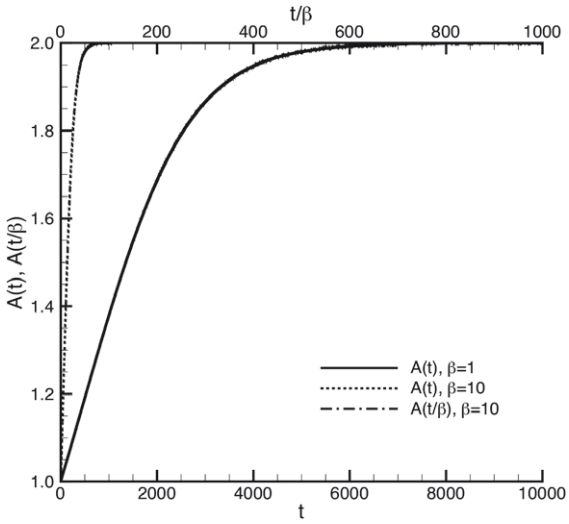

(a) Modeled amplitude

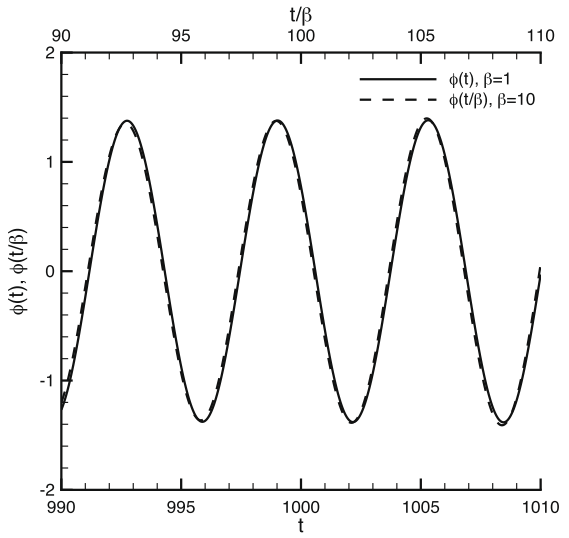

(b) Solution for $t_0/\beta \pm \Delta t$ for $t_0 = 1000$ and $\Delta t = 10$

Fig. 3. Comparison of numerical solutions of van der Pol equation with $\epsilon = 0.001$.

then necessarily a slow derivative, so that an estimate or model of its derivative can be used to estimate the slow derivative of the solution.

In both oscillator examples, the quantity evolving on the slow time scale (the amplitude) was modeled in terms of the solution variables, based on the characteristics of the $\epsilon = 0$ solution. However, imperfections in the straightforward models resulted in residual fast time-scale variations if $\epsilon \neq 0$. They were eliminated by averaging over a period of the fast oscillation, which we again evaluated from the $\epsilon = 0$ solution. The oscillator problems are deterministic, so this approach simply recognizes that the amplitude does not vary with the oscillation of the system, and therefore averaging over the period recovers the same amplitude while eliminating the oscillations introduced by the model imperfections. Similarly, for systems governed by PDEs, one might identify slowly varying quantities that are spatially independent, so that spatial averaging could be used to eliminate rapid variations due to model imperfections.

In more complex systems, such as turbulent fluid flow for example, the solution is stochastic. In turbulence, this is due to uncontrolled small disturbances in initial and boundary conditions. For such systems, the slowly varying quantities will usually be expected values in the relevant probability space. A model for such slow quantities would likely involve time averages over times that are short compared to the long time scale and/or averages in space. One is then assuming that on the short time scale, the system is approximately stationary and ergodic, and in the case of spatial averaging, that the system is spatially homogeneous.

The general approach, then, to modeling the slow derivatives relies on identifying quantities that evolve only on the slow time scale, and developing models for these quantities in terms of solution variables. Unfortunately, it is not possible to be more specific about how such quantities should be identified or modeled, since this will be problem-dependent. This is a modeling task, which requires the physical and mathematical insight of the analyst. This modeling process is exercised in a more complex system, namely an SRM, in the following section.

3. Slow-time acceleration in an SRM

As an example of slow-time acceleration, the fluid dynamics of a solid rocket motor (SRM) are considered. An SRM is a simple device consisting of a chamber lined with solid propellant open to the surroundings through a converging–diverging nozzle. The combustion of the solid propellant produces hot gases that pressurize the chamber and generate thrust as they escape through the nozzle. The basic performance characteristics of an SRM can be analyzed easily by modeling the propellant combustion as simple mass addition and using the quasi-one-dimensional nozzle equations, see Sutton and Biblarz [18]. However, the detailed physics of an SRM are much more complex and include phenomena such as turbulence, multi-phase flow, vortex generation, ignition, flame spread, so-called "erosive" burning, and micro-scale combustion processes, among others. These processes operate on time scales that are much shorter than the long pressurization (volume-filling) and burn-back time scales. The development of the slow-time acceleration modeling approach was prompted by our interest in simulating these fast processes and how they evolve slowly during the operation of an SRM. However, for illustrative purposes, we consider here a simple SRM model (called an idealized SRM here) that does not include these complex physical processes, yet still retains the multiple-time-scale characteristics of an SRM. This makes possible simulations with and without acceleration for the purposes of comparison.

In the simple SRM model considered here, we assume inviscid flow of an ideal gas and represent the propellant combustion by simple mass injection at a specified temperature. As the propellant is consumed, its slow regression changes the geometry of the chamber. As described below, the slow time scales are the volume-filling and propellant-regression time scales, while the fast time scales are the fluid time scales characterizing the equilibration of disturbances across the cross-section of the chamber. These time scales are described briefly below.

3.1. Time scales in an idealized SRM

Here we only discuss the time scales relevant to the idealized SRM model considered here. For a more complete discussion see Haselbacher et al. [9].

The burn-out time scale is given by the thickness of the solid propellant, the so-called web thickness b, divided by the regression rate $\dot{r}$,

$$\tau_{\text{burn}} = \frac{b}{\dot{r}}. \tag{32}$$

The volume-filling time scale is the time scale governing the return to quasi-steady conditions in the chamber following a disturbance (see the appendix for a derivation),

$$\tau_{\text{fill}} = \left(\frac{\gamma+1}{2\gamma}\right)^{\frac{1}{2}} \frac{V}{A_{\text{thr}}\sqrt{RT_0}}, \tag{33}$$

where γ is the ratio of specific heats, V is the chamber volume, A_{thr} is the nozzle throat area, R is the gas constant, and T_0 is the total temperature in the chamber. In SRM, there are a variety of fast time scales. One example is the shear time scale that characterizes the evolution and equilibration of the inviscid solution. The shear time scale can be estimated from

$$\tau_{\text{shear}} = \frac{D_{\text{ch}}}{u}, \tag{34}$$

where D_{ch} is the chamber diameter and u is the centerline axial velocity. Therefore, we have

$$\frac{\tau_{\text{fill}}}{\tau_{\text{shear}}} = \frac{1}{4}\left(\frac{\gamma+1}{2}\right)^{\frac{1}{2}} \frac{A_{\text{inj}}}{A_{\text{thr}}} \frac{u}{a_0}, \tag{35}$$

where A_{inj} is the propellant surface area through which mass, momentum, and energy are injected into the chamber, a_0 is the total speed of sound, and it is assumed that $A_{\text{inj}} = \pi D_{\text{ch}} L$ with L denoting the chamber length. Furthermore,

$$\frac{\tau_{\text{burn}}}{\tau_{\text{fill}}} = \left(\frac{2}{\gamma+1}\right)^{\frac{1}{2}} \frac{b}{L} \frac{A_{\text{thr}}}{A_{\text{ch}}} \frac{a_0}{\dot{r}}, \tag{36}$$

where A_{ch} is the chamber cross-sectional area. For typical values of the relevant parameters, e.g., $b = O(1)$ m, $L = O(10)$ m, $\dot{r} = O(10^{-2})$ m/s, $A_{\text{inj}}/A_{\text{thr}} = O(10^2 - 10^3)$, $A_{\text{thr}}/A_{\text{ch}} = O(10^{-1})$, $u = O(10^2)$ m/s, and $a_0 = O(10^3)$ m/s, one obtains

$$\frac{\tau_{\text{burn}}}{\tau_{\text{fill}}} \gg 1, \tag{37}$$

$$\frac{\tau_{\text{fill}}}{\tau_{\text{shear}}} \gg 1. \tag{38}$$

Therefore, the fast fluid-dynamic time scale indicated in Fig. 1 is the shear time scale. In our SRM simulations reported below, we wish to leave the shear time scale unaffected while accelerating the volume-filling and burn-out time scales.

3.2. Evolution equations

The governing equations are the time-dependent three-dimensional Euler equations in integral form for a control volume V_i with control surface ∂V_i,

$$\frac{d}{dt}\int_{V_i} \mathbf{q} dV + \oint_{\partial V_i} \mathbf{f} ds = \mathbf{0}, \tag{39}$$

where $\mathbf{q}$ represents the state vector of conserved variables and $\mathbf{f}$ is the inviscid flux vector. These vectors can be written as

$$\mathbf{q} = \{\rho, \rho\mathbf{u}, \rho E\}^t, \quad \mathbf{f} = \mathbf{q}(\mathbf{u} - \mathbf{w}) \cdot \mathbf{n} + p\{0, \mathbf{n}, \mathbf{u} \cdot \mathbf{n}\}^t, \tag{40}$$

where ρ is the density, $\mathbf{u} = \{u, v, w\}^t$ is the velocity vector, E is the internal energy per unit mass, $\mathbf{w}$ is the velocity vector of the control surface, $\mathbf{n}$ is the outward unit normal vector to the control surface, and p is the pressure. The ideal gas law is assumed to apply, i.e.,

$$p = (\gamma - 1)\rho\left(E - \frac{1}{2}\|\mathbf{u}\|^2\right), \tag{41}$$

where γ is the ratio of specific heats, assumed to be a constant.

For brevity, the derivation of the governing equations with accelerated slow time scales is based on the general scalar evolution equation,

$$\frac{d}{dt}\int_{V_i} \rho\psi dV = -\oint_{\partial V_i} \rho\psi(\mathbf{u} - \mathbf{w}) \cdot \mathbf{n} ds + \int_{V_i} F(\psi) dV, \tag{42}$$

where ψ is a property per unit mass and $F(\psi)$ is a generic source term. With suitably chosen ψ, the Euler Eq. (39) can be recovered. (In the energy equation, the flux term includes not only the internal energy but also a contribution from the pressure. This additional contribution can be absorbed into $F(\psi)$ and does not alter the analysis.) Putting $\phi = \rho\psi$, where ϕ represents some property per unit volume, and defining the cell-average

$$\phi_i = \frac{1}{V_i}\int_{V_i} \phi dV, \tag{43}$$

gives

$$\frac{d(\phi_i V_i)}{dt} = -\oint_{\partial V_i} \phi(\mathbf{u} - \mathbf{w}) \cdot \mathbf{n} ds + \int_{V_i} F(\phi) dV. \tag{44}$$

In the context of SRM simulations, the propellant surface is represented by an injection boundary moving at the regression velocity $\mathbf{w}$. Because the regression velocity will be modified to accelerate the volume-filling and burn-out time scales, terms involving $\mathbf{w}$ must be isolated. This can be done by using the geometric conservation law (GCL), see, e.g., Thomas and Lombard [19],

$$\frac{dV_i}{dt} = \oint_{\partial V_i} \mathbf{w} \cdot \mathbf{n} ds, \tag{45}$$

so that Eq. (44) can be expressed as

$$V_i \frac{d\phi_i}{dt} = -\oint_{\partial V_i} \phi\mathbf{u} \cdot \mathbf{n} ds + \oint_{\partial V_i} (\phi - \phi_i)\mathbf{w} \cdot \mathbf{n} ds + \int_{V_i} F(\phi) dV. \tag{46}$$

Further development depends on defining the bulk average

$$\overline{\phi} = \frac{1}{D}\sum_i \phi_i V_i, \tag{47}$$

where D is the volume of the entire solution domain and the fluctuation as

$$\phi_i' = \phi_i - \overline{\phi}. \tag{48}$$

The equation describing the evolution of bulk properties is obtained by applying Eq. (46) to the entire solution domain D with boundary ∂D,

$$D\frac{d\overline{\phi}}{dt} = -\oint_{\partial D}\phi\mathbf{u}\cdot\mathbf{n}ds + \oint_{\partial D}(\phi-\overline{\phi})\mathbf{w}\cdot\mathbf{n}ds + \int_D F(\phi)dV. \tag{49}$$

By defining the residuals

$$R_i = \oint_{\partial V_i}\phi\mathbf{u}\cdot\mathbf{n}ds - \int_{V_i}F(\phi)dV, \tag{50}$$

$$\overline{R} = \oint_{\partial D}\phi\mathbf{u}\cdot\mathbf{n}ds - \int_{D}F(\phi)dV, \tag{51}$$

the above equations can be rewritten as

$$V_i\frac{d\phi_i}{dt} = -R_i + \oint_{\partial V_i}(\phi-\phi_i)\mathbf{w}\cdot\mathbf{n}ds, \tag{52}$$

$$D\frac{d\overline{\phi}}{dt} = -\overline{R} + \oint_{\partial D}(\phi-\overline{\phi})\mathbf{w}\cdot\mathbf{n}ds. \tag{53}$$

Therefore, the equation governing the fluctuation is given by

$$V_i\frac{d\phi_i'}{dt} = -R_i' + \oint_{\partial V_i}(\phi-\phi_i)\mathbf{w}\cdot\mathbf{n}ds - \frac{V_i}{D}\oint_{\partial D}(\phi-\overline{\phi})\mathbf{w}\cdot\mathbf{n}ds, \tag{54}$$

where

$$R_i' = R_i - \frac{V_i}{D}\overline{R}. \tag{55}$$

Since the geometry and $\overline{\phi}$ evolve slowly as described in Section 2.1, the goal is to accelerate both by β. Let $T=\epsilon t$ be the slow time scale so that $\phi=\phi(t,T)$ and $\overline{\phi}=\overline{\phi}(T)$ and put $\mathbf{w}=\epsilon\hat{\mathbf{w}}$. (The interpretation of ϵ in the context of SRM simulations is discussed at the end of this section.) Then Eqs. (53) and (54) become

$$D\epsilon\frac{d\overline{\phi}}{dT} = -\overline{R} + \epsilon\oint_{\partial D}(\phi-\overline{\phi})\hat{\mathbf{w}}\cdot\mathbf{n}ds, \tag{56}$$

$$V_i\frac{\partial\phi_i'}{\partial t} + V_i\epsilon\frac{\partial\phi_i'}{\partial T} = -R_i' + \epsilon\oint_{\partial V_i}(\phi-\phi_i)\hat{\mathbf{w}}\cdot\mathbf{n}ds - \epsilon\frac{V_i}{D}\oint_{\partial D}(\phi-\overline{\phi})\hat{\mathbf{w}}\cdot\mathbf{n}ds. \tag{57}$$

As explained in Section 2.1, the goal is to modify Eq. (46) so that when ϵ is replaced by $\beta\epsilon$ the resulting multi-scale equations are identical to Eqs. (56) and (57). The modified form of Eq. (46) is assumed to take the form

$$V_i\frac{d\phi_i}{dt} = -\oint_{\partial V_i}\phi\mathbf{u}\cdot\mathbf{n}ds + \oint_{\partial V_i}(\phi-\phi_i)\mathbf{w}\cdot\mathbf{n}ds + \int_{V_i}F(\phi)dV + S_i, \tag{58}$$

where S_i is a source term to be determined. The corresponding equations for the bulk evolution and the fluctuation are

$$D\frac{d\overline{\phi}}{dt} = -\overline{R} + \oint_{\partial D}(\phi-\overline{\phi})\mathbf{w}\cdot\mathbf{n}ds + \overline{S}, \tag{59}$$

$$V_i\frac{d\phi_i'}{dt} = -R_i' + \oint_{\partial V_i}(\phi-\phi_i)\mathbf{w}\cdot\mathbf{n}ds - \frac{V_i}{D}\oint_{\partial D}(\phi-\overline{\phi})\mathbf{w}\cdot\mathbf{n}ds + S_i', \tag{60}$$

where

$$S_i' = S_i - \frac{V_i}{D}\overline{S}. \tag{61}$$

The multi-scale versions of these equations are

$$D\beta\epsilon\frac{d\overline{\phi}}{dT} = -\overline{R} + \beta\epsilon\oint_{\partial D}(\phi-\overline{\phi})\hat{\mathbf{w}}\cdot\mathbf{n}ds + \overline{S}, \tag{62}$$

$$V_i\frac{\partial\phi_i'}{\partial t} + V_i\beta\epsilon\frac{\partial\phi_i'}{\partial T} = -R_i' + \beta\epsilon\oint_{\partial V_i}(\phi-\phi_i)\hat{\mathbf{w}}\cdot\mathbf{n}ds - \beta\epsilon\frac{V_i}{D}\oint_{\partial D}(\phi-\overline{\phi})\hat{\mathbf{w}}\cdot\mathbf{n}ds + S_i'. \tag{63}$$

By equating Eqs. (56) and (62), it follows that

$$\overline{S} = -(\beta-1)\overline{R}. \tag{64}$$

Eqs. (57) and (63) can be made identical if the terms involving the grid speeds are scaled by β^{-1} and

$$S_i' = (\beta - 1)V_i\epsilon\frac{\partial\phi_i'}{\partial T}. \tag{65}$$

With these modifications, Eqs. (59) and (60) become

$$D\frac{d\overline{\phi}}{dt} = -\beta\overline{R} + \oint_{\partial D}(\phi - \overline{\phi})\mathbf{w}\cdot\mathbf{n}ds, \tag{66}$$

$$V_i\frac{d\phi_i'}{dt} + (1-\beta)V_i\epsilon\frac{\partial\phi_i'}{\partial T} = -R_i' + \frac{1}{\beta}\oint_{\partial V_i}(\phi - \phi_i)\mathbf{w}\cdot\mathbf{n}ds - \frac{1}{\beta}\frac{V_i}{D}\oint_{\partial D}(\phi - \overline{\phi})\mathbf{w}\cdot\mathbf{n}ds, \tag{67}$$

and the equation governing the evolution of ϕ_i is

$$V_i\frac{d\phi_i}{dt} + (1-\beta)V_i\epsilon\frac{\partial\phi_i'}{\partial T} = -\left(R_i + (\beta-1)\frac{V_i}{D}\overline{R}\right) + \frac{1}{\beta}\oint_{\partial V_i}(\phi - \phi_i)\mathbf{w}\cdot\mathbf{n}ds + \frac{\beta-1}{\beta}\frac{V_i}{D}\oint_{\partial D}(\phi - \overline{\phi})\mathbf{w}\cdot\mathbf{n}ds. \tag{68}$$

Note that, having established Eqs. (64) and (65), it is not possible to derive Eq. (68) by computing S_i from Eq. (61). The reason is that by multiplying the grid-speed terms in Eq. (63) by β^{-1}, an inconsistency is introduced because the corresponding term in Eq. (62) was not multiplied by β^{-1}. Therefore, the two terms no longer cancel when summed to derive the evolution equation for ϕ_i.

It is useful to recast Eq. (68) in a form that is more convenient for the implementation in a typical program based on the finite-volume method, i.e., closer to the form of Eq. (44). After some manipulations, the resulting equation can be written as

$$\frac{d(\phi_i V_i)}{dt} = -\mathcal{R}_i + \mathcal{S}_i, \tag{69}$$

where the residual $\mathcal{R}_i$ is

$$\mathcal{R}_i = R_i - \oint_{\partial V_i}\phi\mathbf{w}\cdot\mathbf{n}ds = \oint_{\partial V_i}\phi(\mathbf{u}-\mathbf{w})\cdot\mathbf{n}ds - \int_{V_i}F(\phi)dV, \tag{70}$$

and the source term $\mathcal{S}_i$, which is non-zero only if $\beta > 1$, is

$$\mathcal{S}_i = -(1-\beta)V_i\epsilon\frac{\partial\phi_i'}{\partial T} + \frac{1-\beta}{\beta}\oint_{\partial V_i}(\phi - \phi_i)\mathbf{w}\cdot\mathbf{n}ds - (\beta-1)\frac{V_i}{D}\left(\overline{\mathcal{R}} - \frac{1-\beta}{\beta}\oint_{\partial D}(\phi - \overline{\phi})\mathbf{w}\cdot\mathbf{n}ds\right) - (\beta-1)\frac{V_i}{D}\oint_{\partial D}\overline{\phi}\mathbf{w}\cdot\mathbf{n}ds, \tag{71}$$

with

$$\overline{\mathcal{R}} = \overline{R} - \oint_{\partial D}\phi\mathbf{w}\cdot\mathbf{n}ds. \tag{72}$$

This form suggests an implementation in which the residual is first computed in the same manner as for problems without slow-time acceleration, and then a source term consisting of several correction terms is added.

The small parameter ϵ can be interpreted as the ratio of a fast to a slow time scale, i.e., $\epsilon \sim \tau_f/\tau_s$. Referring to the discussion of the time scales in SRM in Section 3.1, we can take $\epsilon = \tau_{\text{shear}}/\tau_{\text{fill}}$.

3.3. Modeling of slow derivatives

A general feature of the slow-time acceleration approach is that the slow derivatives must be modeled. The slow derivatives were not difficult to model in the simple oscillators described in Section 2.2 because much was known about the solutions. However, the general approach outlined there is commonly applicable. The key idea is to (i) identify quantities that evolve primarily on the slow time scale, (ii) determine how the amplitude of the fast time-scale evolution scales with these slow time-scale quantities, and (iii) estimate the slow time-scale quantities and their derivatives from the overall solution. To illustrate how this modeling approach can be applied to a more complex problem, we explore below several approaches for the SRM problem.

In Eq. (68), the only slow-time derivatives are those of the fluctuations. Here we make the modeling assumption that the dominant slow-time effect is the amplitude evolution of the fluctuations. Then using the general approach employed for the oscillator problems described in Section 2.2, it is assumed that the slow-time derivative of ϕ can be modeled as

$$\frac{\partial\phi'}{\partial T} \approx \frac{1}{A}\frac{dA}{dT}\phi', \tag{73}$$

where A is an amplitude representing the magnitude of the fluctuations. One must then model the logarithmic derivative of A, from information on how the amplitude scales with the slowly varying quantities. In the case of SRMs, the most easily accessible slowly varying quantities are the bulk or volume-averaged variables $\overline{\phi}$. For SRMs with center-perforated grain considered in Section 4.1, the bulk values of the cross-streamwise velocities are zero, and so are their derivatives, of course.

The other bulk properties (density, axial momentum, and total energy) do vary slowly in time, and their slow derivatives can be determined from the numerical solution of Eq. (59). The slow-derivative model would then be obtained by putting $A \sim \overline{\phi}$ in Eq. (73).

However, if the propellant or rocket geometry vary in the axial direction, such as in a star grain (see Section 4.2 and Fig. 8) or in the nozzle, modeling the amplitude variation in terms of the bulk variation may be inadequate. Furthermore, an axial variation in the logarithmic derivative of the amplitude may exist. Then the general approach underlying Eq. (73) is not valid. Several alternative approaches can be envisaged. First, a rather straightforward but powerful approach to estimating an axially-dependent amplitude derivative is to use a quasi-one-dimensional model like that discussed in Section 4.1.1 with spatially-dependent injection and volume information taken from a full three-dimensional simulation. The quasi-one-dimensional problem will be solved orders of magnitude faster than the three-dimensional problem, so it can be run without acceleration and used to estimate the slow derivatives. The only fast time-scale dynamics expected in the quasi-one-dimensional problem are high-wavenumber acoustics. By filtering the solution in space and/or time, the slow derivatives of the cross-sectional averages of density, streamwise momentum, and total energy can be estimated from the one-dimensional solution. Alternatively, instead of solving the quasi-one-dimensional equations, one can simply use these equations to compute the time derivative of the cross-sectionally averaged density, streamwise momentum and total energy based on the cross-sectionally averaged three-dimensional solution. Finally, another approach to computing estimates of the slow derivatives is to determine the derivative of the cross-sectionally averaged and time-filtered solution of the three-dimensional simulations.

The general slow-derivative modeling approaches described above should be usable in many problems, though there is a much broader set of possible slow-evolution behaviors (see Section 2.3). In the simple SRM examples described below, we have focused on the slow-time acceleration implications for the injection boundary conditions because these are in some ways more subtle (see Section 3.4). Because of the simplicity of these problems, it is the boundary treatment that dominates the acceleration model. So in the results described here, the slow derivative in Eq. (68) was neglected. In more complex cases, such as when turbulence effects are included and modeled by large-eddy simulation, for example, a treatment of the slow derivative as described above will be needed.

3.4. Boundary conditions

To complete the description of slow-time acceleration, the effect of the acceleration on the boundary conditions must be determined. In the context of an SRM, injection, solid wall, and outflow boundary conditions are required. Of these, only the injection boundary condition must be investigated because the other two do not depend on the regression rate. At an injection boundary, the mass flux $\dot{m}_{\text{inj}} = \rho(\mathbf{u} - \mathbf{w}) \cdot \mathbf{n}$ and the static temperature T_{inj} are specified and therefore the effect of acceleration on these quantities must be established. Note that $\dot{m}_{\text{inj}}$ is negative by definition.

To determine the effect of slow-time acceleration on the mass flux, Eq. (69) is applied to the overall solution domain D (so $V_i = D,\ R_i = \overline{R}$, and $\mathcal{R}_i = \overline{\mathcal{R}}$), and hence

$$\frac{d\overline{\rho}D}{dt} = -\beta \oint_{\partial D} \rho(\mathbf{u} - \mathbf{w}) \cdot \mathbf{n} ds - (\beta - 1) \oint_{\partial D} \rho \mathbf{w} \cdot \mathbf{n} ds. \tag{74}$$

Using the superscripts n and a to denote nominal and accelerated conditions, the goal of slow-time acceleration can be expressed as

$$\left(\frac{d\overline{\rho}D}{dt}\right)^a = \beta \left(\frac{d\overline{\rho}D}{dt}\right)^n, \tag{75}$$

or

$$-\beta \oint_{\partial D} \dot{m}^a_{\text{inj}} ds - (\beta - 1) \oint_{\partial D} \rho \mathbf{w}^a \cdot \mathbf{n} ds = -\beta \oint_{\partial D} \dot{m}^n_{\text{inj}} ds, \tag{76}$$

from which the desired relationship between the accelerated and nominal mass fluxes is extracted as

$$\dot{m}^a_{\text{inj}} = \dot{m}^n_{\text{inj}} - \frac{\beta - 1}{\beta} \rho \mathbf{w}^a \cdot \mathbf{n}. \tag{77}$$

Because $\mathbf{w} \cdot \mathbf{n} > 0$ on injection boundaries, accelerating the regression rate increases the magnitude of the injection mass flux.

A similar analysis for the energy equation leads to the result that the injection temperature is not changed by slow-time acceleration, i.e., $T^a_{\text{inj}} = T^n_{\text{inj}}$.

4. Results

The results presented below were obtained by numerically solving the time-dependent quasi-one-dimensional and three-dimensional Euler equations. In contrast to typical formulations of the quasi-one-dimensional Euler equations, see, e.g., Toro

[21], the form adopted in the present work does not explicitly involve the cross-sectional area. Instead, only the pressure term is considered for the control-volume faces that are not perpendicular to the streamwise coordinate. This allows the quasi-one-dimensional equations to be written in the form of Eq. (42).

As stated in Section 3.1, the effects of turbulence, multi-phase flow, and other complex phenomena are neglected for simplicity. Therefore, the fast fluid-dynamic time scale is the shear time scale given by Eq. (34) that characterizes the evolution and equilibration of the inviscid solution. In the quasi-one-dimensional simulation reported in Section 4.1.1below, this time scale is not present. But the approach is still valid and is pursued in this case to demonstrate the capabilities of the method. Slow-time acceleration is applied to three-dimensional rocket simulations, in which the shear time scale is important, in Sections 4.1.2 and 4.2.

In the simulations reported below, the grids are moving and deforming in response to the regression of the solid propellant. A discrete version of the GCL given by Eq. (45) is satisfied to ensure that the grid motion does not induce spurious sources of mass, momentum, and energy. In all cases, the initial conditions are atmospheric values for pressure and temperature and zero velocity. The entire propellant surface is assumed to ignite instantaneously.

4.1. Generic motor with center-perforated grain

A so-called center-perforated grain configuration is investigated first. This axisymmetric geometry is characterized by mass injection through a cylindrical surface. A schematic illustration of a cross-section of such a configuration is shown in Fig. 4. In a center-perforated grain configuration, the surface area through which mass is injected increases with time as the propellant is consumed and therefore the head-end pressure increases also. The configuration considered here had a chamber length of 3.81 m, chamber diameter of 0.381 m, and a throat diameter of 0.172 m. The regression rate and injection mass flux without acceleration were $5 \cdot 10^{-3}$ m/s and 8.513 kg/(m^2 s), respectively. The injection temperature was 3000 K. The gas constant and the ratio of specific heats were 325.97 J/(kg K) and 1.2144, respectively. Both quasi-one-dimensional and three-dimensional computations were carried out for this configuration.

4.1.1. Quasi-one-dimensional simulations

Using the quasi-one-dimensional code described above, the impact of the acceleration parameter β on the solution accuracy relative to a simulation without acceleration was investigated.

The computations with acceleration $\beta > 1$ were restarted at a physical time of 5 s from a computation carried out with $\beta = 1$. The effect of the acceleration parameter on the head-end pressure is shown in Fig. 5(a). The head-end pressure decreases slightly with increasing β at a fixed time, but the difference remains approximately constant at only 0.01 %. For the temperature at the head end, increasing β also leads to a slight underprediction relative to $\beta = 1$, but again the differences are very small, as may be observed from Fig. 5(b). Interestingly, small-amplitude transient oscillations can be observed in the solution, whose period appears to increase with increasing β. The origin of these oscillations is not known at present.

The effect of the acceleration parameter on the axial variations of the static pressure and velocity is shown in Fig. 5(c) and (d). Increasing values of β lead to underprediction of the pressure, but the differences are small. The velocity appears to be almost completely unaffected by changes of the acceleration parameter.

4.1.2. Three-dimensional simulations

The three-dimensional computations were carried out with a unstructured-grid computational-fluid-dynamics code developed at CSAR, see, e.g., Haselbacher [6,7] and Haselbacher and Najjar[8]. The grids used in these computations consisted of 85836 tetrahedra. The injection temperature was 2856 K.

A comparison of the head-end pressure as a function of time for slow-time acceleration with $\beta = 50$ and no acceleration is shown in Fig. 6. At present, the slow-time acceleration method is only implemented in serial (although the overall code can be run in parallel), so that explicit computations are very expensive for the reasons explained above. For this reason, while

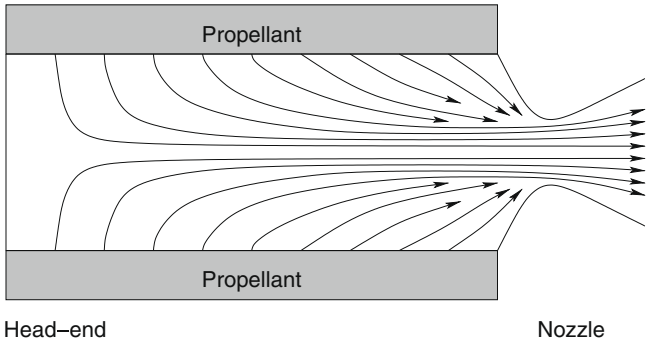

Fig. 4. Cross-section of center-perforated rocket configuration considered in Section 4.1. The arrows represent schematic depictions of streamlines.

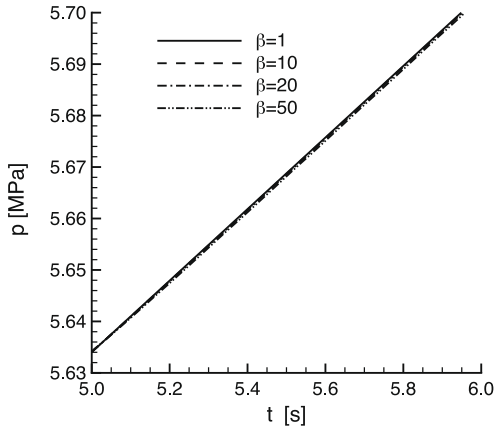

(a) Effect of acceleration parameter on head-end pressure. Inset shows detail view.

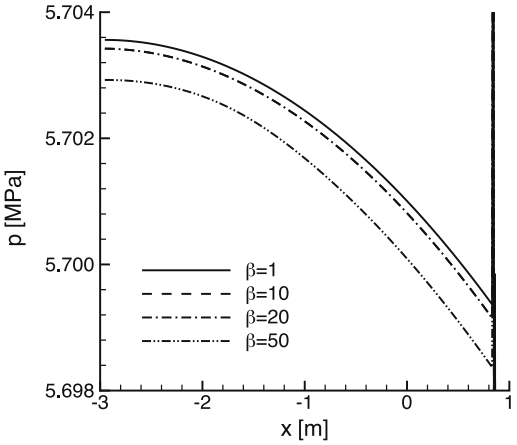

(c) Effect of acceleration parameter on pressure along axis.

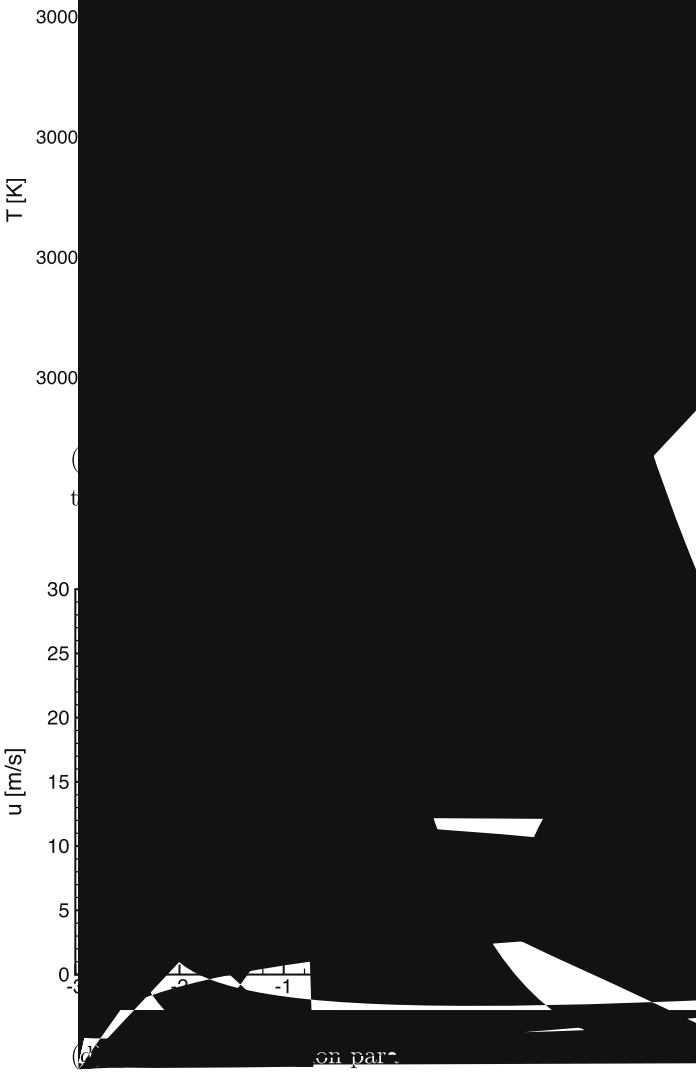

the computation with slow-time acceleration was run until close to burn-out, the computation without slow-time acceleration was only run until the beginning of quasi-steady state conditions. As can be seen from Fig. 6(a), the overall agreement between the computations with and without slow-time acceleration is good until the end of the latter. As indicated by the arrows in Fig. 6(a) the computation with slow-time acceleration reached about 6.2 s of physical time in about 80 h, while the computation without acceleration reached about 0.34 s of physical time in about 159 h. Thus an actual speed-up of about 36.2 in CPU time is obtained with an acceleration parameter of $\beta = 50$. The discrepancy between the acceleration parameter and the actually obtained acceleration is due to the need to compute bulk variables and the additional terms on the right-hand side of Eq. (69). A more detailed comparison, depicted in Fig. 6(b), reveals the close agreement between the computations with and without slow-time acceleration. Again, transient oscillations appear in the pressure following the activation of the acceleration. The cause of the oscillations is currently unclear.

A comparison of the solution along the axis is shown in Fig. 6(c) and (d). The acceleration of the slow time scale has no appreciable effect on the pressure and velocity along the axis, as desired.

4.2. Generic motor with star grain

The slow-time acceleration approach was also applied to three-dimensional simulations of geometrically more complex SRM configurations. In the example shown below, the motor exhibits a so-called star grain configuration near the head-end, i.e., the cross section is a six-pointed star, see Fig. 8. The propellant structures with primarily radial extent are usually

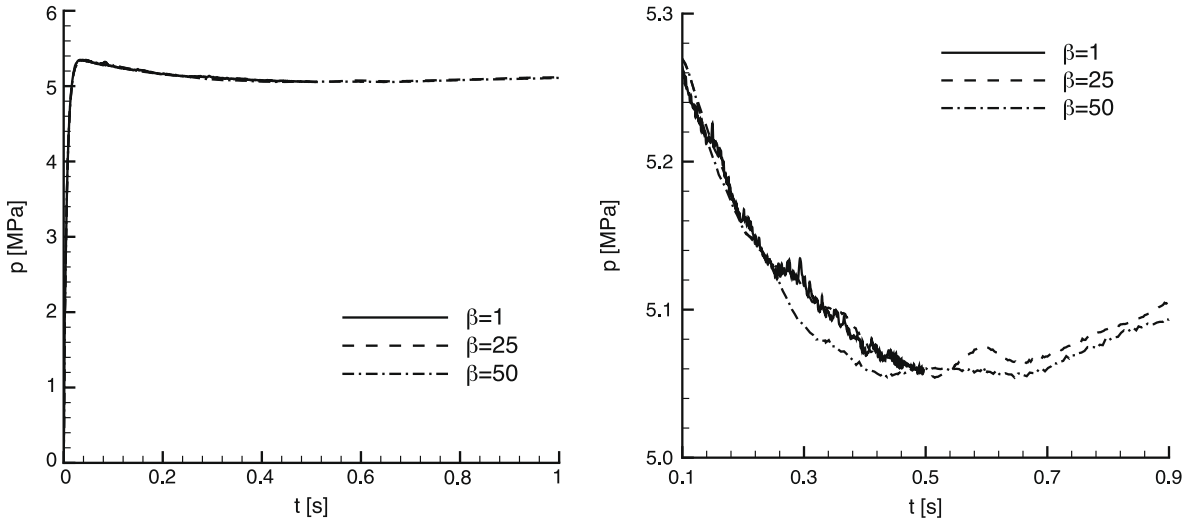

(a) Head-end pressure. (b) Detail view of head-end pressure.

Fig. 7. Results for three-dimensional simulations of motor with star grain.

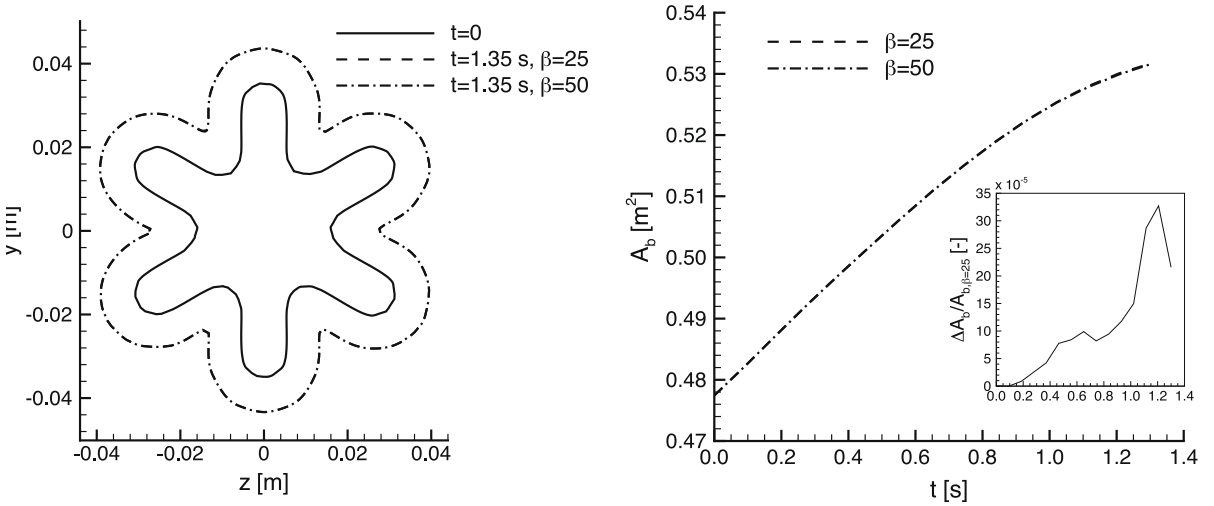

(a) Comparison of cross-sections at $x = 0.97$ m. (b) Comparison of surface areas. Inset shows relative differenc between surface areas.

Fig. 8. Evolution of propellant surface in three-dimensional simulations of motor with star grain.

Fig. 7(b). The magnitude of the burn-back at $x = 0.97$ m after $t = 1.35$ s is presented in Fig. 8(a). The predicted propellant burn-back is very similar for both values of the acceleration parameter. A comparison of the surface area as a function of time for $\beta = 25$ and 50 is presented in Fig. 8(b). The normalized difference, shown in the inset, is $O(10^{-4})$. These results demonstrate that the slow-time acceleration approach performs well in non-trivial three-dimensional geometries also.

5. Discussion and generalizations

In this paper, the problem of numerically simulating the dynamics of systems with disparate time scales was addressed through an approximation technique based on multi-scale asymptotics. The fundamental problem facing such simulations is that their cost scales like τ_s/τ_f, where τ_s and τ_f are the slowest and fastest time scales in the system, respectively. When the time scales differ by many orders of magnitude, this cost can be prohibitive.

The treatment of such multiple-time-scale problems necessarily depends on which time scales are of primary interest. In some situations, for example, one is primarily interested in evolution on the slow time scale. In this case, approximations

based on homogenization of the fast scales and/or quasi-equilibrium of the fast-scale dynamics are appropriate, see, e.g., Holmes [10]. Chemically reacting systems with widely varying reaction rates are a good example of this type of multiple-time-scale problem. Another common example is a spurious fast time-scale introduced by the spatial discretization. The use of implicit time discretizations to avoid stability constraints can be interpreted as a quasi-equilibrium treatment of the spurious fast time scale.

The slow-time acceleration approach presented here for use in the SRM problem addresses the opposite and often more challenging situation in which the fast-scale dynamics are of primary interest. It is also useful when the fast-scale dynamics are sufficiently complex that models are not available for their homogenized effects. SRMs are a good example of the former, and a maneuvering aircraft is an example of the latter (the fluid-dynamic time scales are fast compared to the vehicle dynamics). In either case, we seek to reduce τ_s/τ_f and thus the simulation cost, while preserving an accurate representation of both the slow and fast-scale dynamics.

In the case of SRMs, the anomalously slow time scales associated with regression of the propellant surface and volume filling/pressurization, were much slower than the next slowest time scales. In general, this would allow a multi-scale asymptotic representation of the system, in which the time-scale ratio is the small parameter. However, in the slow-time acceleration technique, this representation is not followed. Instead, modified equations are derived that have the same multi-scale asymptotic form as the original equations when the slow time scales are accelerated. This approach is general in its applicability, requiring only the separation in time scales discussed above. However, to close the resulting slow-time accelerated equations, a model will generally be needed for the slow-time derivatives. Thus, the slow-time acceleration technique introduces an asymptotic error and a modeling error.

When applied to SRM computations, it was found that slow-time acceleration allowed detailed simulations of an entire burn in a factor of 36 shorter simulation time. Tests showed that quantities that evolve on the slow time scale, such as the head-end pressure, were very accurately reproduced by the accelerated system. Furthermore, at any given time, details of the solution that evolve on the fast time scale, such as spatial variation of the pressure or velocity, were well represented in the slow-time accelerated simulations. In short, the target capability of accurate short and long time-scale dynamics in a significantly cheaper simulation was attained.

However, the acceleration of slow time scales requires some care in the interpretation of simulation results, since the definition of time depends, in essence, on the context. For example, in the SRM problem, if one is interested in the nature of the flow one second after ignition, one must interrogate the solution at $t = 1/\beta$ seconds of simulation time, since the slow time has been accelerated by a factor of β. And, if one is interested in vortex-shedding dynamics (from an inhibitor, say, see Sutton and Biblarz [18] and Anthoine et al. [1]) one second after ignition, this will correspond to the simulated evolution (at the simulating time scale) evaluated again at $t = 1/\beta$ seconds, but the variation of these dynamics (e.g., changes in shedding frequency) will occur β times faster.

While the slow-time acceleration technique proposed here was developed for use in SRM simulations, it is clearly applicable to a wide variety of problems with anomalously slow time scales. As such, it is a valuable addition to our simulation tools for multi-scale problems. In its current formulation, the slow-time acceleration technique works by accelerating a set of slow time scales (the burn-back and volume-filling time scales in the SRM application) by the same factor. However, as is clear from Fig. 1, there may also be a large disparity between the scales that are being accelerated. It would be useful to generalize the formulation so that different slow scales can be accelerated by different factors. For example, referring to Fig. 1, it should be possible to accelerate the burn-back time scale by a much larger factor than the volume-filling time scale, while maintaining a significant separation between the scales. Further development is needed in this area.

Acknowledgments

The work reported here was carried out while the authors were at the Center for Simulation of Advanced Rockets at the University of Illinois at Urbana-Champaign. The Center for Simulation of Advanced Rockets is supported by the Department of Energy through the University of California under subcontract number B523819.

Appendix A. Estimation of volume-filling time scale

The objective is to estimate the time scale required for steady or quasi-steady conditions to be established in the chamber following a disturbance. Because the primary interest is in the behavior of the chamber as a whole, the estimation of the volume-filling time scale is based on the mass balance.

Assuming the rate of volume change to be small, the mass balance can be expressed as

$$\frac{d\rho}{dt} = -\frac{1}{V}(\dot{m}_{\text{inj}}A_{\text{inj}} + \dot{m}_{\text{thr}}A_{\text{thr}}), \tag{78}$$

where V is the chamber volume, $\dot{m}_{\text{inj}}$ is the injection mass flux, $\dot{m}_{\text{thr}}$ is the mass flux at the throat, A_{inj} is the injection area, and A_{thr} is the throat area. The density is decomposed as $\rho = \rho_0 + \delta\rho$ with ρ_0 assumed a constant. Furthermore, it is assumed that $\dot{m}_{\text{inj}}$ does not depend on ρ and that the nozzle is choked, so $\dot{m}_{\text{thr}} = \rho^* a^*$ where a is the speed of sound and the superscript $*$

denotes sonic conditions. Using standard compressible-flow relationships, see Thompson [20], it is a simple matter to show that

$$\frac{d\delta\rho}{dt} = \alpha - \frac{\delta\rho}{\tau_{\text{fill}}}, \tag{79}$$

where

$$\alpha = -\frac{1}{V}\left[\dot{m}_{\text{inj}}A_{\text{inj}} + \rho_0\sqrt{RT_0}A_{\text{thr}}\left(\frac{2\gamma}{\gamma+1}\right)^{\frac{1}{2}}\right], \tag{80}$$

and τ_{fill} is the desired volume-filling time scale,

$$\tau_{\text{fill}} = \left(\frac{\gamma+1}{2\gamma}\right)^{\frac{1}{2}}\frac{V}{A_{\text{thr}}\sqrt{RT_0}}, \tag{81}$$

where γ is the ratio of specific heats, R is the gas constant, and T_0 is the total temperature. Under steady-state conditions, $\alpha = 0$.

For the purpose of estimating the volume-filling time scale, the total temperature may be replaced by the injection temperature.

References

[1] J. Anthoine, P. Planquart, D. Olivari, Cold flow investigation of the flow acoustic coupling in solid propellant rockets, AIAA Paper 98-0475, 36th AIAA Aerospace Sciences Meeting and Exhibit, Reno, NV, 1998.
[2] C. Bender, S. Orszag, Advanced Mathematical Methods for Scientists and Engineers, Springer, 1999.
[3] J. Best, The fluid dynamics of river dunes: a review and some future research directions, J. Geophys. Res. 110 (F04S02) (2005) 1–2.
[4] W. Dick, M. Heath, R. Fiedler, M. Brandyberry, Advanced simulation of solid propellant rockets from first principles, AIAA Paper 2005-3990, 41st AIAA/ASME/SAE/ASEE Joint Propulsion Conference, Tucson, AZ, 2005.
[5] J. Ferry, S. Balachandar, A fast Eulerian method for disperse two-phase flow, Int. J. Multiphase Flow 27 (7) (2001) 1199–1226.
[6] A. Haselbacher, A WENO reconstruction algorithm for unstructured grids based on explicit stencil construction, AIAA Paper 2005-0879, 43rd AIAA Aerospace Sciences Meeting and Exhibit, Reno, NV, 2005.
[7] A. Haselbacher, On constrained reconstruction operators, AIAA Paper 2006-1274, 44th AIAA Aerospace Sciences Meeting and Exhibit, Reno, NV, 2006.
[8] A. Haselbacher, F. Najjar, Multiphase flow simulations of solid-propellant rocket motors on unstructured grids, AIAA Paper 2006-1292, 44th AIAA Aerospace Sciences Meeting and Exhibit, Reno, NV, 2006.
[9] A. Haselbacher, F. Najjar, L. Massa, R. Moser, Enabling three-dimensional unsteady SRM burn-out computations by slow-time acceleration, AIAA Paper 2006-4591, 42nd AIAA/ASME/SAE/ASEE Joint Propulsion Conference, Sacramento, CA, 2006.
[10] M. Holmes, Introduction to Perturbation Methods, Springer, 1995.
[11] A. Jameson, Time dependent calculations using multigrid, with applications to unsteady flows past airfoils, AIAA Paper 91-1546, 10th AIAA Computational Fluid Dynamics Conference, Honolulu, HI, 1991.
[12] A. Majda, J. Sethian, The derivation and numerical solution of the equations for zero Mach number combustion, Combust. Sci. Technol. 42 (1985) 185–205.
[13] F. Najjar, J. Ferry, A. Haselbacher, S. Balachandar, Simulations of solid-propellant rockets: effects of aluminum droplet size distribution, J. Spacecraft Rockets 43 (6) (2006) 1258–1270.
[14] V. Pande, I. Baker, J. Chapman, S. Elmer, S. Khaliq, S. Larson, Y. Rhee, M. Shirts, C. Snow, E. Sorin, B. Zagrovic, Atomistic protein folding simulations on the submillisecond time scale using worldwide distributed computing, Biopolymers 68 (1) (2003) 91–109.
[15] T. Pulliam, Time accuracy and implicit methods, AIAA Paper 93-3360, 11th AIAA Computational Fluid Dynamics Conference, Orlando, FL, 1993.
[16] R. Rehm, H. Baum, The equations of motion for thermally driven, buoyant flows, J. Res. Nat. Bur. Stand. 83 (3) (1978) 297–308.
[17] P. Spalart, Direct simulation of a turbulent boundary layer up to $r_\theta = 1410$, J. Fluid Mech. 187 (1988) 61–98.
[18] G. Sutton, O. Biblarz, Rocket Propulsion Elements, seventh ed., Wiley-Interscience, 2000.
[19] P. Thomas, C. Lombard, Geometric conservation law and its application to flow computations on moving grids, AIAA J. 17 (10) (1979) 1030–1037.
[20] P. Thompson, Compressible-Fluid Dynamics, McGraw-Hill, 1972.
[21] E. Toro, Riemann Solvers and Numerical Methods for Fluid Dynamics, second ed., Springer, 1999.
[22] E. Turkel, Preconditioning techniques in computational fluid dynamics, Ann. Rev. Fluid Mech. 31 (1999) 385–416.
[23] P. Venugopal, R. Moser, F. Najjar, Direct numerical simulation of turbulence in injection-driven plane channel flows, Phys. Fluids 20 (10) (2008) 105103.